Quasi-static and dynamic characterization of unidirectional non-crimp carbon fiber fabric composites processed by HP-RTM

Aleksandr Cherniaev[1,2], Yu Zeng[1], Duane Cronin[1], John Montesano[1]*

[1] Department of Mechanical & Mechatronics Engineering, University of Waterloo, 200 University Ave. West, Waterloo, ON, Canada N2L 3G1

[2] Department of Mechanical, Automotive and Materials Engineering, University of Windsor, 401 Sunset Ave., Windsor, ON, Canada N9B 3P4

[*] Corresponding Author Email: john.montesano@uwaterloo.ca

Abstract

Recently developed high-pressure resin transfer molding (HP-RTM) processes have enabled the integration of lightweight fiber-reinforced composites into automobiles (e.g., frame and roof components, floor segments), which may also be suitable for energy absorption applications such as front crush structures in high volume production vehicles. Heavy tow stitch-bonded non-crimp fabrics with rapid curing resins have been recently used to fabricate HP-RTM parts; however, there is a lack of mechanical property data in the literature for such materials. To fill this gap and support the development of lightweight automotive structures, this study reports an investigation assessing the microstructure, quasi-static and dynamic mechanical properties of a non-crimp carbon fabric composite manufactured by HP-RTM, as well as properties of the rapid curing neat epoxy resin. The presented study of the microstructure and constituent properties provide data for in-depth microstructural modeling of the processed non-crimp fabric HP-RTM composite. The study reports 18-20% increase in the tensile transverse strength and strain-at-failure at strain rates on the order of 1000 s^{-1}. Measured macroscopic material properties can be used as input

data for numerical modeling of automotive composite structures, including simulations of vehicle collisions.

Keywords: HIGH PRESSURE RESIN TRANSFER MOLDING (HP-RTM), NON-CRIMP CARBON FABRIC, MECHANICAL PROPERTIES, HIGH STRAIN-RATE CHARACTERIZATION, SPLIT-HOPKINSON BAR

1. Introduction

Recent studies indicate that automobiles account for about one-quarter of overall carbon dioxide emissions, a major contributor to the greenhouse effect [1]. A strategic approach to reducing the fuel consumption and, therefore, CO_2 emissions, is reducing the weight of automobiles through the use of lightweight materials. In this regard, composites, such as plastics reinforced by continuous carbon fibers, have been identified as key materials for enabling substantial weight reductions in mass produced vehicles [2]. As a result of high specific strength and stiffness, these materials allow significant weight savings when used to replace metals in frame parts, roof, and floor segments, as well as many other automobile components [3-6]. In addition, carbon-fiber composites may provide higher passenger safety owing to better energy dissipation capabilities in case of collision, as compared with conventional metallic materials [7-10]. Energy is dissipated in these materials through multiple failure mechanisms, such as delamination, fiber breakage, matrix cracking, and fiber microbuckling [11–14, 35–37]. To support the development of automotive energy absorbing structures (e.g., front crush rails or B-pillars), in addition to assessing quasi-static properties, characterization of high strain-rate behavior of composites is important.

Several studies have reported the strain rate dependent properties of unidirectional CFRP composites. Ploeckl et al. [15] a 40% increase of longitudinal compressive strength at strain rates of 100 s^{-1} was reported for IM7/8552. For the same material system, a 45% increase of transverse

compressive strength and 42% increase of in-plane shear strength at strain rates over 200 s^{-1} was reported in [16]. Melin and Asp [17] studied the effects of strain rate on the transverse tensile properties of a unidirectional CFRP, reporting that the elastic properties were not dependent on the strain rate while the transverse tensile strength was only slightly influenced. Similar trends for transverse tension were reported in [18, 19]. In general, most reported studies consider the strain rate dependence on compressive properties, while few studies report strain rate dependence on tensile properties. In contrast, this study focuses on investigating the transverse tensile strength strain-rate sensitivity of the relatively new type of composite materials – stitch-bonded non-crimp fabric reinforced polymers, which can be distinct from conventional unidirectional composites owing to their different microstructure and employed manufacturing process.

For the manufacturing process, until recently the main challenge of using continuous-fiber composites in high volume production vehicles was a lack of a sufficiently rapid fabrication techniques. Process times for conventional manufacturing techniques (e.g. vacuum bagging, autoclave molding, standard RTM, etc.) usually exceeds minutes or, more often, hours [20]. However, newly developed high-pressure resin transfer molding (HP-RTM) processes along with novel rapid curing resin systems, may enable the integration of composites into vehicles while maintaining the volume production rates typical for the automotive industry. Curing of a composite part can be completed within less than one minute with HP-RTM process [21, 22]. Unidirectional stitch-bonded fabrics are a preferred type of reinforcement for HP-RTM process, as they allow for a rapid build-up of part thickness and preforming capabilities when a binder is used.

Despite of the growing importance of HP-RTM for automotive industry, there is currently a lack of experimental data in the literature for composites fabricated by this manufacturing process, particularly for non-crimp fabric reinforced plastics, including both quasi-static and high strain-rate properties. In order to fill this gap, this paper presents an investigation into microstructure and mechanical performance of a rapid curing thermoset resin composite reinforced by continuous

UD non-crimp carbon fiber fabric and manufactured using HP-RTM process. Such data can be used as input parameters for numerical models of automotive composite structures, including models for car crash simulations. Also, this study reports mechanical properties of the neat epoxy resin fabricated using the same process and used as a matrix of the CFRP composite. This data, along with the presented microscopy analysis, has a potential application in the development of numerical models where mesoscale representation of the composite is required for higher fidelity.

2. Materials and manufacturing

ZOLTEK™ PX35 UD300 unidirectional fabric was used as a reinforcement in this study. The fabric is produced from 50K continuous tow carbon fiber and, as per manufacturer data, has areal density of 333 g/m^2. The fibers in the tows are spread to achieve dry fabric thickness of approximately 0.37 mm and tows are stitched with a polyester stitch in a tricot pattern. Fig. 1 exemplifies the design of the used unidirectional fabric which also has a thermosetting binder applied. An automated cutting center was used for precise cutting of carbon UD fabric.

As a matrix, a fast-cure epoxy system EPIKOTE™ Resin TRAC 06150 in combination with a hardener EPIKURE™ Curing Agent TRAC 06150 and internal mold release agent HELOXY™ Additive TRAC 06805, was used in this study. This three-part system is specifically designed by HEXION® for mass-production of automotive structural parts and has the curing time of 5-10 min [23]. The corresponding mixing ratios used were 100:24:1.2 parts by weight for the resin, hardener and internal release agent.

Traditional resin transfer molding is a slow process: the final part may take hours or days to cure and may require the use of an autoclave to increase production time. However, HP-RTM is designed to impregnate the preform in a few seconds such that highly reactive polymer systems can be used and cured within minutes. In this study, the HP-RTM equipment used consisted of a

high flow injection system (KraussMaffei) combined with a 2,500-ton hydraulic press (Dieffenbacher) to maintain mold closure, both shown in Fig 2.

During the manufacturing cycle resin and hardener were combined at high pressure of 120 bar and injected under vacuum at high flow rate (40 g/s) into a closed mold containing dry UD fabric. Press forces applied to the mold varied from 1500 kN during the injection to 4500 kN during curing. The constant mold temperature was equal to 120 °C. The mold itself, as well as the manufactured panel are shown in Fig. 3. The fabricated flat panel contained 7 layers of UD fabric, which were aligned, in terms of the fiber direction, with the long side of the panel.

In addition to the composite panels, neat resin panels were fabricated in separate trials. The three-part resin system was processed into 4 mm-thick neat resin panels using the HP-RTM setup (Fig. 2) and similar processing parameters as for the composite panels (mold temperature of 120°C and press force of 1000 kN during the injection to 3000 kN during curing).

After manufacturing, it was found that the neat resin panels were slightly curved in the regions near the edges (Fig. 4). Correspondingly, prior to fabricating the test specimens, the panels we flattened by placement into an air-circulated oven and heat was applied with a rate of 5°C/minute up to 120°C, which is near the glass transition temperature of the epoxy. The hot panels were then removed from the oven, placed between two heavy flat steel plates and allowed to cool to room temperature.

3. Experimental methods

Experimental techniques employed in this study for characterization of the materials' microstructure, quasi-static and high strain-rate properties are subsequently detailed.

The microstructure of the composite was studied using KEYENCE opto-digital microscope equipped with the VH-Z500R high-resolution zoom lens (500-5000X). In addition to the visual

investigation of the material's microstructure, digital image recognition tools of the microscope allowed for measurement of constituents' volume fractions.

Quasi-static ($\dot{\varepsilon} \approx 0.01$ s^{-1}) *testing* of the composite and its matrix have been carried out in a constant temperature (24°C±1°C) lab environment using two different test frames. In particular, neat resin properties were determined using an MTS FlexTest SE servo-hydraulic test frame, where the applied force was measured by an external load cell with 2.2 kN capacity. The geometry of the test specimens adopted a modified dog-bone shape (see Fig. 5) that in previous studies was found to provide good agreement with the results obtained using ASTM type V specimens [24]. Due to high longitudinal strength of the carbon fiber composite, this material was tested using a 90 kN servo-hydraulic test frame. The quasi-static tests were conducted according to the ASTM D3039 M standard [25] for the longitudinal tensile and transverse tensile properties. For shear properties characterization, the 10° off-axis tensile test was employed [26]. Specimens for the tests were waterjet-cut from the manufactured panel (Fig. 6), where shorter samples (40mm and 45 mm-long) were used in the high strain-rate testing, as will be discussed below.

Strain measurements for quasi-static tests were performed using the 2D digital image correlation (DIC) technique, which included applying a stochastic speckle pattern on the surface of the specimen (Fig. 7), recording the deformed specimen surface with a high precision optical camera (Nikon D3200 DSLR camera fitted with a Sigma 105 mm f/2.8 macro lens) and post-processing the recorded images using the GOM Correlate software to measure strain. Test setup with the 90 kN machine and the optical camera is exemplified in Fig. 8. For illumination, a lighting kit consisting of two fluorescent lamps was used (Fig. 8). Facet size of 19 x 19 pixels with the point distance of 16 pixels was employed for the DIC analyses, while filtering of undesired data was ensured by setting the admissible deviation of brightness within the facets to 20 gray levels. Verification of the chosen set of DIC parameters was conducted by means of comparison of

determined material properties with data provided by the manufacturer, as described in Section 4.2.

High strain rate testing of the composite material was conducted using the split-Hopkinson tensile bar (SHTB) apparatus at the University of Waterloo (Fig. 9, see also [28]). The SHTB uses a gas gun to propel a concentric hollow striker towards an end cap located at the free end of the incident pressure bar. Upon impact, a generated tensile incident loading pulse travels towards the specimen. As the incident wave reaches the specimen, a portion of it is transmitted into the sample, causing it to deform at high strain rates, with the remainder being reflected. Strain gauges placed on the incident and transmitter bars measure the incident, reflected and transmitted waves (Fig. 10). The waves are then analyzed using standard Hopkinson bar equations to determine the stresses and strain rates experienced by the sample. A detailed description of the split-Hopkinson bar technique can be found in Ref. [29]. In all high strain-rate tests, strains were determined using digital image correlation VIC-2D software from the Photron SA5 high-speed camera output. DIC settings used for high strain-rate experiments were the same as those described above for the quasi-static tests. Used speckle pattern is exemplified in Fig 7. For illumination, a high-power monolight kit shown in Fig. 9 and Fig. 11 was employed in all high strain-rate tests.

Two groups of specimens, different in terms of length only, were cut from the composite panel as (40 mm and 45 mm-long specimens in Fig. 6). As strain rate in SHB experiments is inversely proportional to the length of samples, using specimens of different length allowed to vary strain rates in the tests without additional adjustment of equipment parameters. In the following, shorter samples will be referred to as SHBS and longer ones as SHBL specimens. Test setup for the SHTB experiments is exemplified in Fig. 9. For clamping, specimens were bonded into the 16 mm-long slots in the incident and transmitter bars (see Fig. 9), which produced the unsupported gauge length of 8 mm and 13 mm for SHBS and SHBL specimens, correspondingly.

In order to better understand the observed increase of the ultimate tensile stress of the composite in the matrix-dominated transverse direction, an additional set of experiments was conducted at increased strain rates with the neat epoxy resin. Due to the impedance mismatch of the resin and bars, it was not possible to conduct split-Hopkinson bar tests with the neat epoxy specimens with the same SHTB apparatus used in testing of the composite. Instead, the epoxy was tested using the hydraulic intermediate strain rate (HISR) apparatus at the strain rate corresponding to approximately 24 s^{-1}. Test setup for the neat epoxy specimens is shown in Fig. 11.

4. Results and discussion

4.1 Microstructural characterization

Fig. 12 shows the main characteristic features of the material, including individual tows, resin-rich zones between them and polyester stitching. The material had average tow width of 4.1 mm and tow height of 0.43 mm. The microstructure features 0.14 mm-thick (on average) resin-rich layers between the tows in adjacent plies and thick resin pockets between tows of the same ply.

The in-tow fiber volume fraction was measured using the digital image recognition tools of the microscope. For these measurements, five “control areas” were isolated at different locations in the same laminate. The areas themselves, as well as the calculated fiber volume fractions corresponding to each of them are shown in Fig. 13, while red marks in Fig. 12 show the approximate positions of the control areas on the laminate view. The average in-tow fiber volume fraction was determined as being equal to 0.554, or 55.4%. It should be noted that because of the thick resin-rich layers (Fig. 12), the average volume fraction of fibers in the composite is significantly lower than the measured in-tow value and corresponds to 45%.

It was expected due to the high polymer matrix content that the composite could exhibit strain-rate sensitivity of the matrix-dominant properties, such as transverse tensile strength and

transverse tensile strain-at-failure. Testing of the material at high strain rates is discussed in Section 4.3 of the paper.

4.2 Quasi-static properties

Stress-strain curves obtained in the quasi-static tests of the composite are shown in Fig. 14. The corresponding unidirectional ply properties, as well as the standard deviation, are presented in Table 1. As shown in Fig.14a, the tensile response along the fiber direction is linear elastic as expected due to the ideally non-crimp unidirectional reinforcing fibers. Along the matrix-dominated transverse direction, the response is only slightly nonlinear (see Fig. 14c) which is distinct from the tensile response of the resin (Fig. 16). In contrast, the in-plane shear response beyond an initial elastic range is notably inelastic with > 5% strain at failure as shown in Fig. 14d, which is consistent with unidirectional CFRPs.

It should be noted that in the off-axis tensile tests, as per methodology described in [26], shear strain at any load during the test can be calculated as a function of strains measured on gauges of either a rectangular or a 60-degree strain gauge rosette. To ensure consistency of the calculations, strains in the first off-axis specimen were analyses using both types of rosettes. The rosettes were constructed in the DIC software, as shown in Fig. 15. As expected, both rosettes provided similar predictions of the shear strain values (Fig. 15, center). Correspondingly, only the rectangular rosette was used for strain analysis for the remaining off-axis specimens.

In order to ensure consistency of the results and to verify adequacy of the chosen data processing parameters (e.g., DIC parameters), some of the material properties obtained in this study were compared with the corresponding properties provided by the fabric manufacturer [27]. In particular, longitudinal tensile modulus and longitudinal tensile strength, which are known to scale almost linearly with volume fraction of fibers (v_f) as $E_1 \approx E_f \cdot v_f$ and $X_t \approx \sigma_f \cdot v_f$, were compared. Scaled down from the manufacturer-tested material with $v_f = 0.55$ to the material considered in

this study (v_f = 0.45), these properties can be approximated as E_1 = 97400 MPa and X_t = 1145 MPa, which is within 5% agreement with the values presented in Table 1.

To enhance understanding of the composite behavior in matrix-dominant directions, as well as to support future development of the mesoscopic computational models of the non-crimp fabric reinforced composite, the neat resin matrix was also characterized in this study. The resulting tensile engineering stress-engineering strain diagrams for the tested neat resin demonstrates low variability (Fig. 16, Table 2). The observed response of the material correlated well with the behavior of this and other similar epoxy resins described in the literature (see e.g. [30, 31]), where a clear transition from elastic to inelastic behavior occurred with notable elongation at failure.

4.3 High strain-rate properties

Only strain rate sensitivity of the composite material along the matrix-dominated transverse direction under tensile loading was studied in this work. The strain rates in the tests were relatively constant and the average measured values for shorter (SHBS) and longer (SHBL) samples were equal to 1925 and 1230 s^{-1}, correspondingly. Several consecutive images recorded by the high-speed camera during one of the tests are shown in Fig. 17. Formation of the longitudinal (with respect to fiber direction) crack and stitching pullout are noticeable in the high-speed imagery. All tested samples exhibited the failure in the vicinity of the bars (by the gage length), as shown in Fig. 9 and 17. Measured values of the tensile transverse strength and transverse strain-at-failure of the composite material are provided in Table 3-4 and also shown graphically in Fig. 18.

As can be deduced from presented data, the material exhibits strain-rate sensitivity along the matrix-dominant transverse direction. Despite the limited number of tests conducted and noticeable scatter in the results, the mean values of the composite's transverse tensile strengths at strain rates of 1230 s^{-1} and 1925 s^{-1} are approximately 18% and 20% higher than the

corresponding value measured in the quasi-static experiments. For the transverse tensile strain-at-failure, approximately 19% increase at high strain-rates can be reported.

It should also be noted that all specimens tested at high strain rates failed in the vicinity of the constrained ends, where stress concentration is most likely present. Therefore, it may be expected that increase of the transverse strength and strain-at-failure of the material with strain rate can be even more pronounced than reported in this study. As a result, the reported values should be considered as the lower-boundary estimates of the transverse tensile properties of the material at the corresponding strain rates.

For the neat epoxy specimens tested at the rate of approximately 24 s^{-1}, resulting stress-strain diagrams are shown in Fig. 19. Average value of the ultimate tensile stress of the epoxy obtained in these tests corresponded to 112 ± 4 MPa (the particular source of uncertainty is unknown, however a possible reason for variation of the measured ultimate stresses can be associated with uncertainty of force measurement in these dynamic experiments), which is about 23% higher as compared with the quasi-static value reported in Section 4.2 for this material. Similar trends have been reported by other researchers for epoxy resins in [32, 33]. It can, therefore, be concluded that the strain-rate sensitivity of epoxy resin coupled with the existence of the large resin-rich zones between fiber tows (see Fig. 12) may be significant contributors to the overall strain-rate sensitivity of the non-crimp carbon fabric-reinforced composite along the transverse direction. However, presence of high fraction of the strain-rate non-sensitive fibers expectedly limits the strain rate sensitivity of the CFRP when compared to that of the resin. Also, it should be recalled that the high strain rate dependency observed for the studied non-crimp fabric material along the tensile transverse direction was not observed for similar UD composites from the literature [17-19] and may be a distinct property of the non-crimp fabric which is an important finding of this study. In addition, the use of an internal mold release in the resin formulation, which is typical for a rapid HP-RTM process, may also contribute to the enhanced strain rate dependency of both

the neat resin and the CFRP material studied. A recent study [34] has shown that internal mold release can influence the properties of carbon fiber epoxy materials.

7. Conclusions

This paper presented results of an investigation into the microstructure, quasi-static properties and strain rate dependent mechanical response of an epoxy resin composite reinforced by continuous non-crimp unidirectional fabric manufactured using an HP-RTM process.

The in-plane mechanical properties of the non-crimp fabric composite were first obtained at quasi-static loading conditions and represent the material parameters required by most macroscale material models for numerical (e.g. finite element) analysis of composite structures. This data is supplemented with the analysis of microstructure of the material and quasi-static properties of its constituent (neat epoxy resin) which can be used in the development of the numerical models with the mesoscale representation of the composite.

In addition, the transverse tensile strength of the composite material and transverse tensile strain-at-failure were characterized at high strain-rates using a split-Hopkinson bar apparatus. These matrix-dominant properties were chosen for the high strain-rate characterization owing to the measured strain-rate sensitivity of the studied epoxy from corresponding dynamic tests and the large resin-rich zones observed between fiber tows in the composite as determined by the microscopy analysis. Based on the limited number of high strain-rate experiments presented, it can be preliminarily concluded that the studied composite material exhibits, as compared with the quasi-static properties, approximately 18-20% increase in the tensile transverse strength and strain-at-failure at strain rates on the order of 1000 s^{-1}. This notable strain rate sensitivity in tension along the transverse fiber direction is distinct from that reported in other studies for unidirectional composites, and may be a distinct characteristic of stitch-bonded non-crimp fabric reinforced polymers which is a key finding of this study. Also, the generated dynamic test data can be used

to support the development of numerical models for crash simulations involving composite parts fabricated by HP-RTM process.

Acknowledgements

The authors would like to thank the Natural Sciences and Engineering Research Council of Canada (NSERC) for financial support through Collaborative Research and Development Grant No. CRDPJ 507776 – 16, as well as sponsors from Honda R&D Americas, Hexion Inc., Zoltek Corp. and LAVAL International. Amir Zhumagulov and Jose Imbert-Boyd (University of Waterloo) are also acknowledged for supporting the conducted experiments. The Fraunhofer Project Center for Composites Research (Canada) is also acknowledged for fabricating the panels.

References

1. Drivers and Impacts of Greenhouse Gas Emissions, Environment and Climate Change Canada, Apr. 13, 2017, https://www.canada.ca/en/environment-climate-change/services/environmental-indicators/greenhouse-gas-emissions-drivers-impacts.html (accessed on Dec. 11, 2018)
2. Kelly J.C., Sullivan J.L., Burnham A., Elgowain A. Impacts of Vehicle Weight Reduction via Material Substitution on Life-Cycle Greenhouse Gas Emissions, Environment Science and Technology, 49 (2015) 12535-1254
3. Davies G., Materials for Automobile Bodies, Elsevier, Oxford (2000)
4. Brooks R., Shanmuga Ramanan S.M., Arun S. Composites in Automotive Applications: Design, In Reference Module in Materials Science and Materials Engineering, Elsevier, 2017.
5. Komus A., Beley N. Composite Applications for Ground Transportation, In Reference Module in Materials Science and Materials Engineering, Elsevier (2017)
6. Ning H., Pillay S., Vaidya U.K. Design and development of thermoplastic composite roof door for mass transit bus, Materials & Design, Volume 30, Issue 4 (2009) 983-991
7. Guangyong Sun, Shunfeng Li, Qiang Liu, Guangyao Li, Qing Li, Experimental study on crashworthiness of empty/aluminum foam/honeycomb-filled CFRP tubes, Compos. Struct. 152 (2016) 969–993
8. Guohua Zhu, Guangyong Sun, Qiang Liu, Guangyao Li, Qing Li, On crushing characteristics of different configurations of metal-composites hybrid tubes, Compos. Struct. 175 (2017) 58–69.
9. Guohua Zhu, Guangyong Sun, Hang Yu, Shunfeng Li, Qing Li, Energy absorption of metal, composite and metal/composite hybrid structures under oblique crushing loading, Int. J. Mech. Sci. (2018) 458–483
10. Guangyong Sun, Zhen Wang, Jiaying Hong, Kai Song, Qing Li, Experimental investigation of the quasi-static axial crushing behavior of filament-wound CFRP and aluminum/CFRP hybrid tubes, Compos. Struct. (2018)

11. Lu G., Yu T. X. Energy Absorption of Structures and Materials, 1st Edition. Woodhead Publishing, (2003)
12. Mamalis A.G., Robinson M., Manolakos D.E., Demosthenous G.A., Ioannidis M.B., Carruthers J. Crashworthy capability of composite material structures, Composite Structures, Volume 37, Issue 2 (1997) 109-134
13. Mamalis A.G., Manolakos D.E., Ioannidis M.B., Papapostolou D.P. On the crushing response of composite sandwich panels subjected to edgewise compression: experimental, Composite Structures, 71 (2005) 246-257.
14. Huang W.C., Cha C.S., Yang I.Y. Optimal crashworthiness design of CFRP hat shaped section member under axial impact, Mater. Res. Innovations, 15 (2011)
15. Marina Ploeckl, Peter Kuhn, J.ürgen Grosser, Markus Wolfahrt, Hannes Koerber, A dynamic test methodology for analyzing the strain-rate effect on the longitudinal compressive behavior of fiber-reinforced composites, Compos. Struct. 180 (2017) 429–438
16. H. Koerber, J. Xavier, P.P. Camanho, High strain rate characterisation of unidirectional carbon-epoxy IM7-8552 in transverse compression and in-plane shear using digital image correlation, Mech. Mater. 42 (11) (2010) 1004–1019
17. G. Melin, L., E. Asp, L. Effects of strain rate on transverse tension properties of a carbon/epoxy composite: studied by moiré photography. Composites Part A: Applied Science and Manufacturing, 30(3), (1999) 305–316.
18. Weeks C.A., Sun C.T. Modeling non-linear rate-dependent behaviour in fiber-reinforced composites. Composites Science and Technology, 58 (1998) 603-611
19. Gilat A., Goldberg R.K., Roberts G.D. Experimental study of strain-rate-dependent behaviour of carbon/epoxy composite. Composites Science and Technology, Volume 62 (2002) 1469-1476
20. Mazumdar S. Composites Manufacturing: Materials, Product, and Process Engineering, CRC Press (2001)
21. Fais C. Lightweight automotive design with HP-RTM, Reinforced Plastics, Volume 55, Issue 5 (2011) 29-31
22. COMPOSITES EUROPE highlights solutions for mass production of automotive composites, Reinforced Plastics, Volume 55, Issue 4, 2011, Pages 45-46.
23. https://www.hexion.com/en-AU/applications/composites/automotive/structural/ (accessed on Dec. 11, 2018)
24. Trimino L.F., Cronin D., Evaluation of numerical methods to model structural adhesive response and failure in tension and shear loading, J. Dynamic Behavior Mater, 2 (2016) 122–137.
25. ASTM. Standard test method for tensile properties of polymer matrix composite materials, annual book of ASTM standard. West Conshohocken (PA): ASTM (2017). ASTM D3039/D3039M – 17.
26. Chamis C.C, Sinclair J.H. 10 deg. off-axis tensile test for intralaminar shear characterization of fiber composites. NASA TN D-8215 (1976)
27. http://zoltek.com/wp-content/uploads/2017/09/TDS_PX35_Uni-Directional_Fabrics.pdf (accessed on Dec. 11, 2018)
28. Smerd R., Winkler S., Salisbury C., Worswick M.J., Lloyd D., Finn M. High strain rate tensile testing of automotive aluminum alloy sheet. Int J Impact Eng, 32 (1–4) (2005), 541-560
29. Meyers MA. Dynamic behavior of materials. John Wiley & Sons Inc (1994)

30. Vita A., Castorani V., Germani M. Manufacturing, process simulation and mechanical tests of a thick component produced by Compression-RTM process. In: Proceedings of ECCM18 - 18th European Conference on Composite Materials Athens, Greece, 24-28th June 2018.
31. Littell J.D., Ruggeri C.R., Goldberg R.K., Roberts G.D., Arnold W.A., Binienda W.K. Measurement of Epoxy Resin Tension, Compression, and Shear Stress–Strain Curves over a Wide Range of Strain Rates Using Small Test Specimens. Journal of Aerospace Engineering (2008)
32. Gerlach R., Siviour C.R., Petrinic N., Wiegand J. Experimental characterisation and constitutive modelling of RTM-6 resin under impact loading, Polymer 49 (2008) 2728–2737
33. Tamrakar S., Ganesh R., Sockalingam S., Haque B.Z., Gillespie J.W. Experimental investigation of strain rate and temperature dependent response of an epoxy resin undergoing large deformation, Journal of Dynamic Behavior of Materials, 4 (2018) 114–128
34. Rich M.J., Askeland P., Drown E., Drzal L.T. Surface and interfacial engineering of fast curing epoxy/carbon fiber composites. Society of Plastic Engineers Automotive Composites Conference and Exhibition (SPE ACCE), Novi, Michigan, Sep. 5-7, 2018.
35. Patel J, Peralta P. Mechanisms for Kink Band Evolution in Polymer Matrix Composites: A Digital Image Correlation and Finite Element Study. ASME. ASME International Mechanical Engineering Congress and Exposition, Volume 9: Mechanics of Solids, Structures and Fluids; NDE, Diagnosis, and Prognosis (2016), pp 1-12. doi:10.1115/IMECE2016-67482
36. Budiansky B., Fleck N.A., Compressive failure of fibre composites, Mech Phys Solids, 41 (1) (1993), 183-211.
37. Moran P., Shih C., Kink band propagation and broadening in ductile matrix fiber composites: experiments and analysis, Int J Solids Struct, 35 (15) (1998), 1709-1722.

Figure Captions

Fig.1. Unidirectional CFRP fabric PX35 UD300 (scale in mm)

Fig.2. Manufacturing equipment used to fabricate composite panels: HP-RTM line (left); hydraulic press (right)

Fig.3. Flat mold (left) and a manufactured panel (right)

Fig.4. Neat resin panel with the edges curved in manufacturing

Fig.5. Neat resin tensile test specimen

Fig.6. Dimensions and cutting directions of the specimens with respect to the panel and manufactured specimens for mechanical testing

Fig.7. Test setup for the quasi-static experiments

Fig.8. Split-Hopkinson tensile bar apparatus and tested composite specimen

Fig.9. Incident, transmitted and reflected pulses recorded by strain gages of the split-Hopkinson bar

Fig.10. Setup for the intermediate strain-rate tests of the neat epoxy

Fig.11. Optical images showing the microstructure of the UD fabric CFRP composite

Fig.12. Microstructural images used for in-tow fiber volume fraction measurements

Fig.13. Loading curves for the composite specimens: a) longitudinal tension stress-strain curves; b) strain-time for longitudinal and transverse directions for Poisson ratio measurement; c) transverse tension stress-strain curve; d) stress-strain curves for the off axis tensile tests

Fig.14. Off-axis tensile test: shear strain measurement (rectangular and 60-degree rosettes) and specimen failure mode

Fig.15. Stress-strain diagrams for neat epoxy specimens tested at the intermediate strain rate of 24 s-1 (curves in the figure correspond to five specimens tested at the same conditions)

Fig.16. Failure of a composite sample loaded along transverse direction, recorded by the high-speed camera

Fig.17. Transverse strength (left) and transverse strain-at-failure (right) of the composite as a function of strain rate ("min" and "max" correspond to the minimum and maximum values observed in the experiments; "x" represents the mean value)

Fig.18. Uniaxial tensile test stress-strain diagrams for the neat resin specimens

Tables

Table 1 – Measured unidirectional ply properties

Property	Mean value	Standard deviation
Longitudinal Young's modulus E_1, MPa	102665	3769
Transverse Young's modulus E_2, MPa	8109	170.7
Major in-plane Poisson's ratio ν_{12}, –	0.253	0.007
In-plane shear modulus G_{12}, MPa	3095	113
Longitudinal tensile strength X_t, MPa	1204	50.1
Transverse tensile strength Y_t, MPa	51.9	5.0
In-plane shear strength S_L, MPa	65.3	1.3
Longitudinal strain-at-failure ε_{1f}, %	1.175	0.09
Transverse strain-at-failure ε_{2f}, %	0.694	0.10
In-plane shear strain-at-failure γ_{12f}, %	5.357	0.26

Table 2 – Measured properties of the neat epoxy

Property	Mean value	Standard deviation
Young's modulus E, MPa	3080	50
0.2% offset yield stress σ_Y, MPa	46.66	1.73
Poisson's ratio ν, –	0.39	0.01
Ultimate tensile strength σ_{UTS}, MPa	85.76	0.65
Strain at ultimate tensile strength ε_{UTS}, %	7.16	0.31
Strain at failure ε_F, %	8.15	1.11

Table 3 – Measured tensile transverse strength of the composite at different strain rates

	Test 1 (MPa)	Test 2 (MPa)	Test 3 (MPa)	Mean (MPa)	Std. Dev (MPa)	CV, %
QS	46.43	56.31	52.91	51.88	5.02	9.67

SHBL (1230 s^{-1})	65.14	56.98	61.86	61.33	4.11	6.70
SHBS (1925 s^{-1})	60.96	54.13	71.72	62.27	8.87	14.24

Table 4 – Measured tensile transverse strain-at-failure of the composite at different strain rates

	Test 1 (%)	Test 2 (%)	Test 3 (%)	Mean (%)	Std. Dev (%)	CV, %
QS	0.585	0.711	0.787	0.694	0.10	14.69
SHBL (1230 s^{-1})	0.965	0.847	0.726	0.846	0.12	14.13
SHBS (1925 s^{-1})	0.793	0.851	0.771	0.805	0.04	5.13

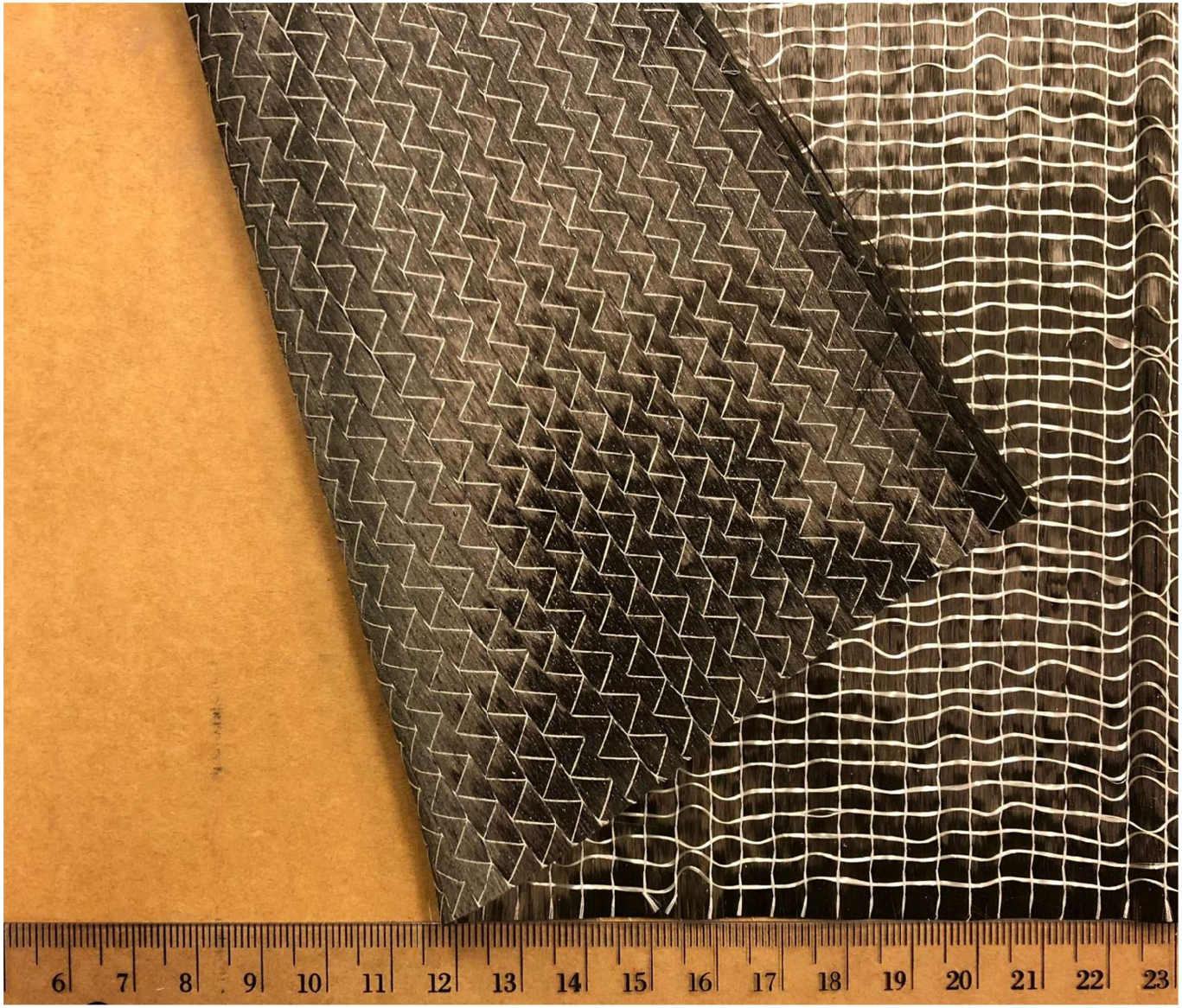
6
7
8
9
10
11
12
13
14
15
16
17
18
19
20
21
22
23


DIEFFENBACHER

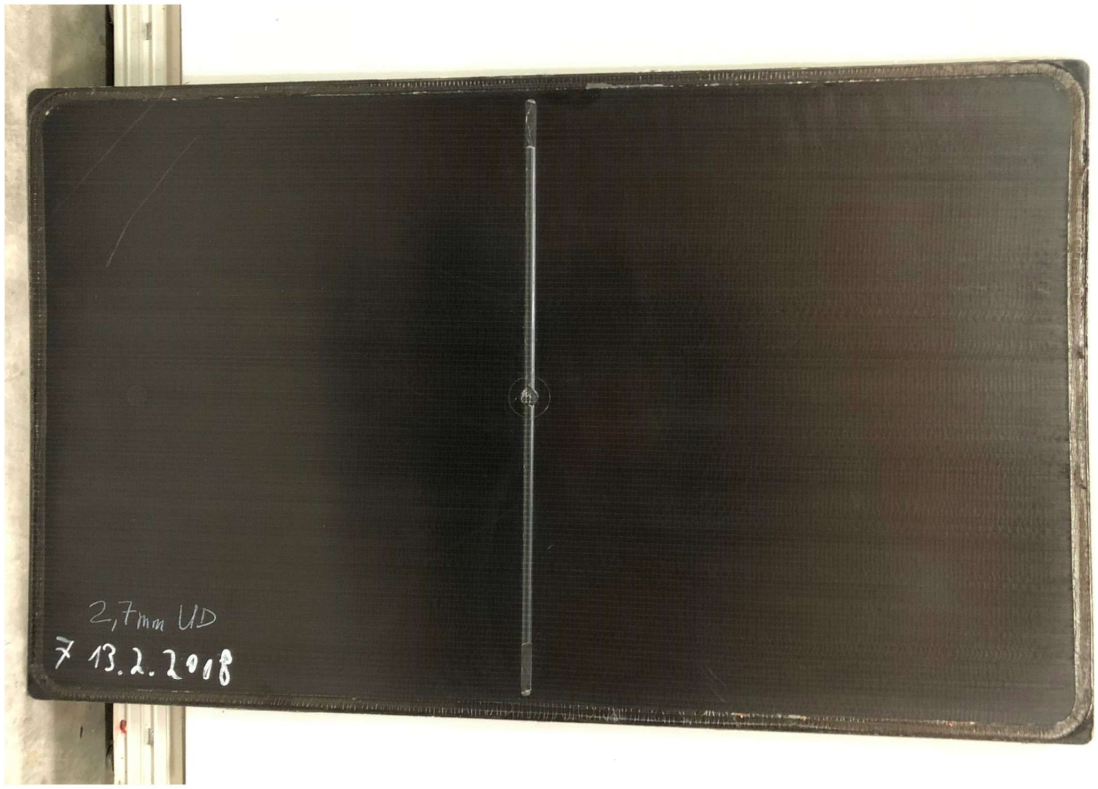
2,7mm UD
13.2.2018

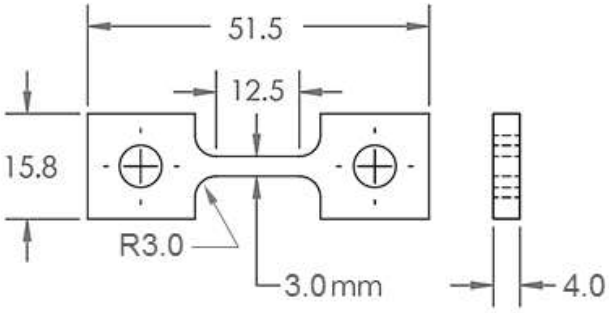
51.5
12.5
15.8
R3.0
3.0mm
4.0

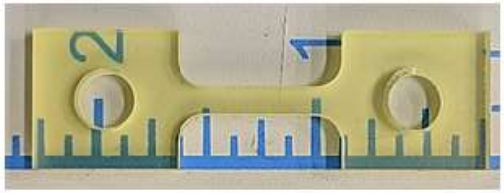

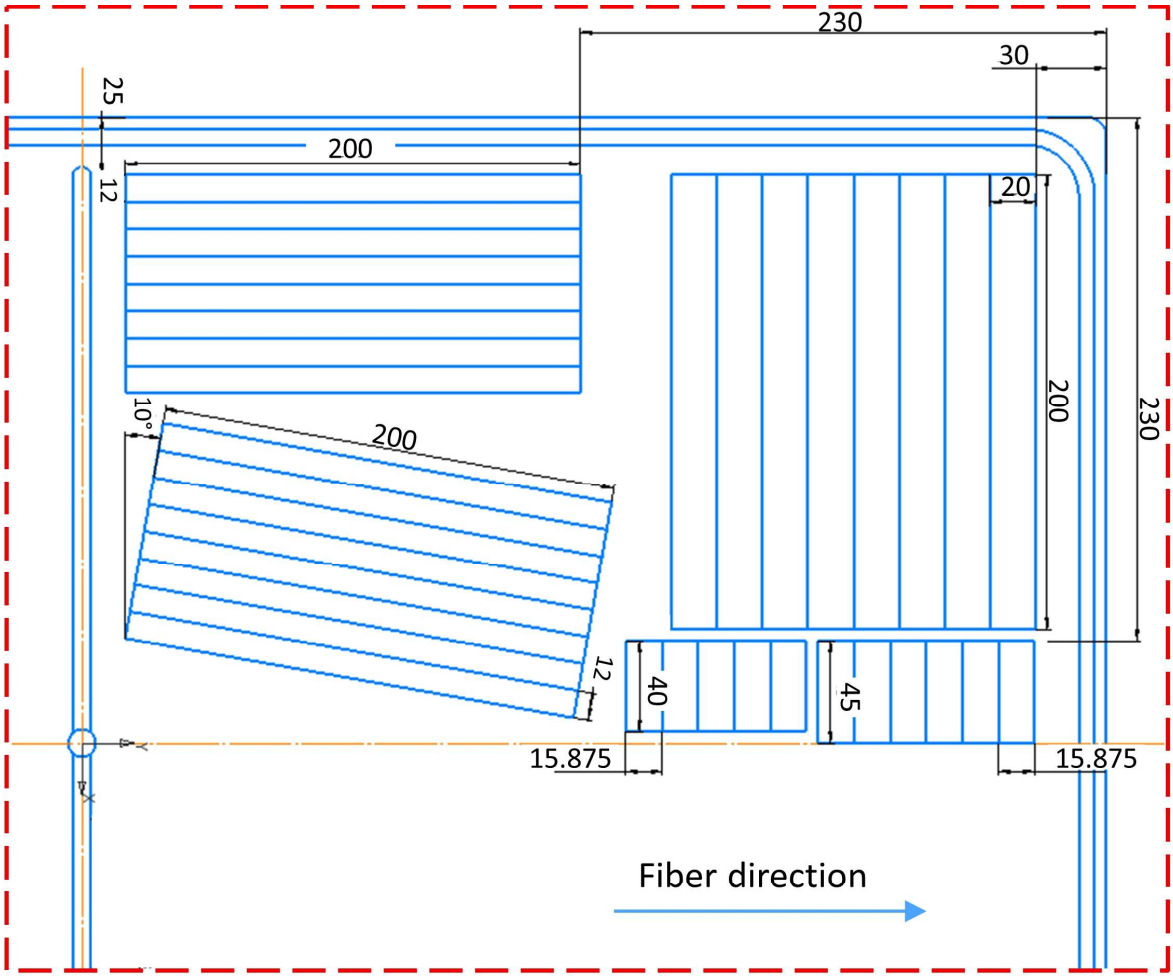
230
30
25
200
12
20
200
230
10°
200
12
40
45
15.875
15.875
Fiber direction

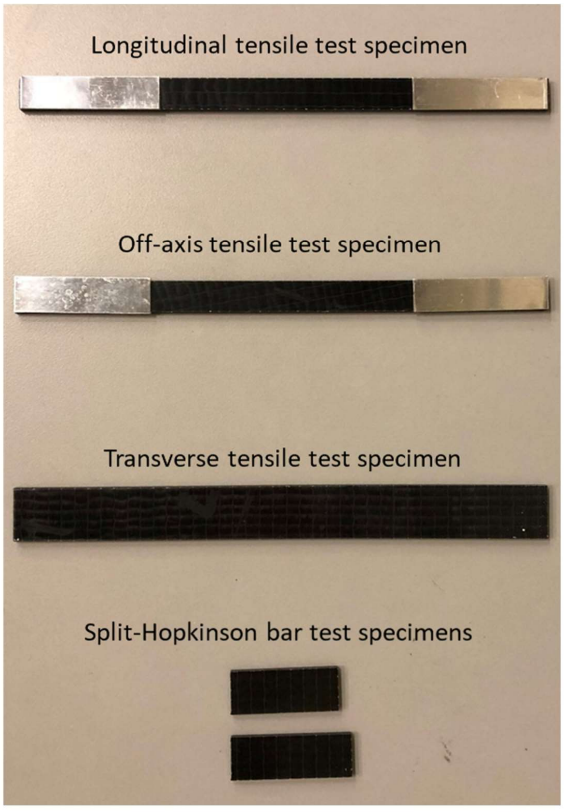
Longitudinal tensile test specimen
Off-axis tensile test specimen
Transverse tensile test specimen
Split-Hopkinson bar test specimens

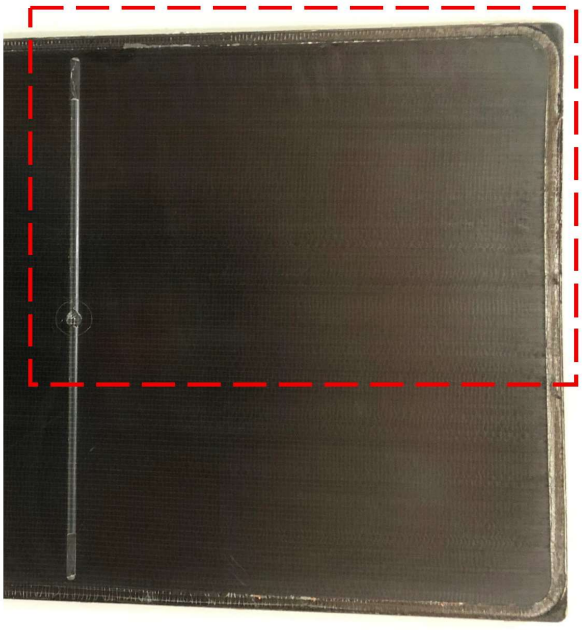

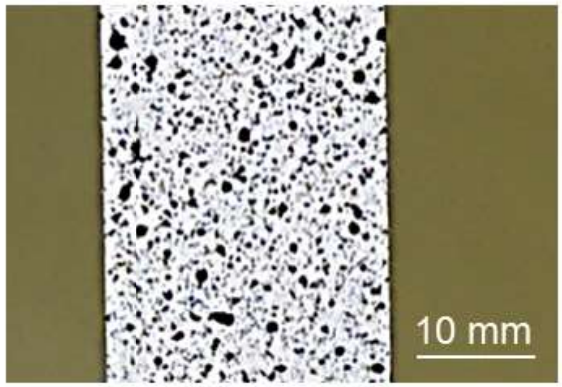
10 mm

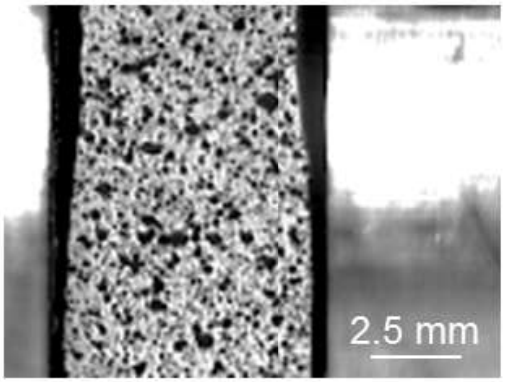
2.5 mm

acer

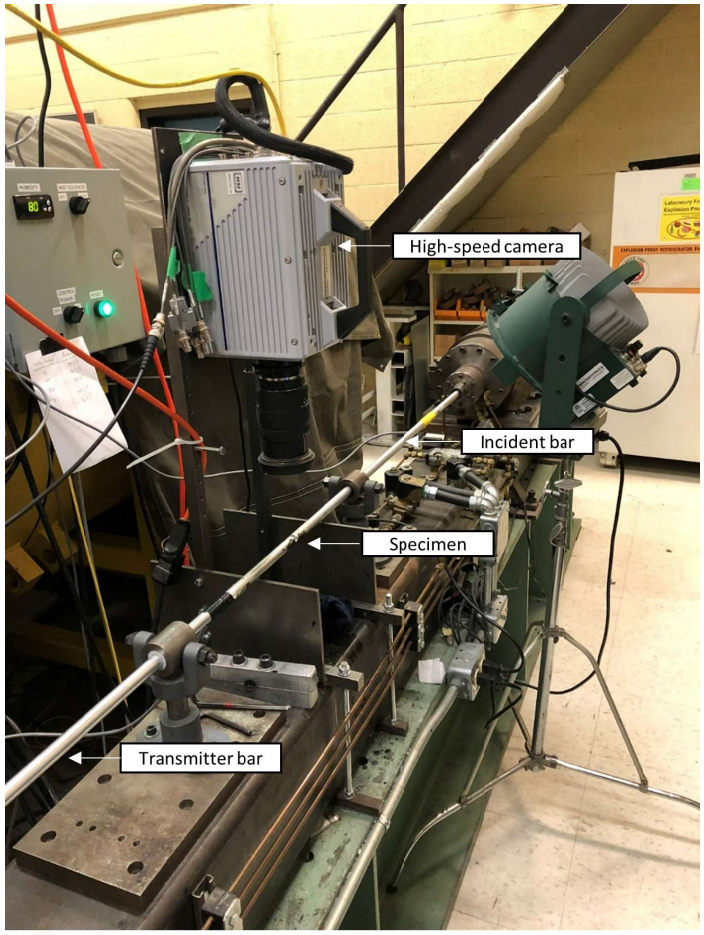
High-speed camera
Incident bar
Specimen
Transmitter bar

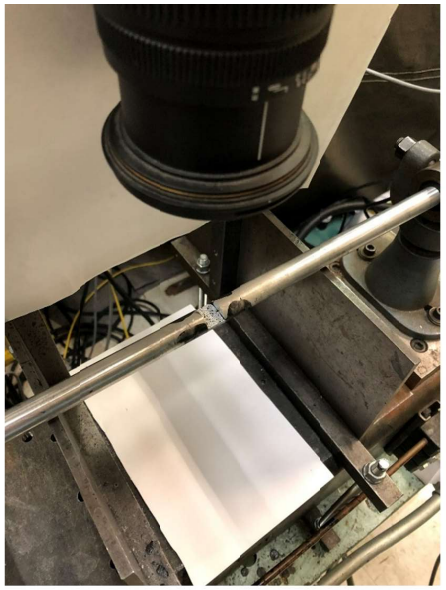

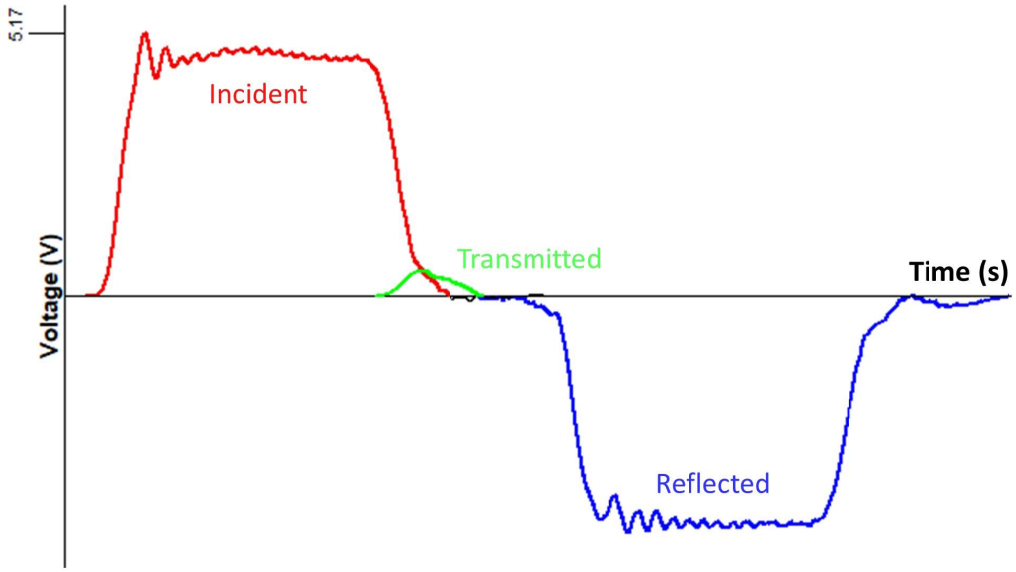
5.17
Incident
Transmitted
Time (s)
Voltage (V)
Reflected

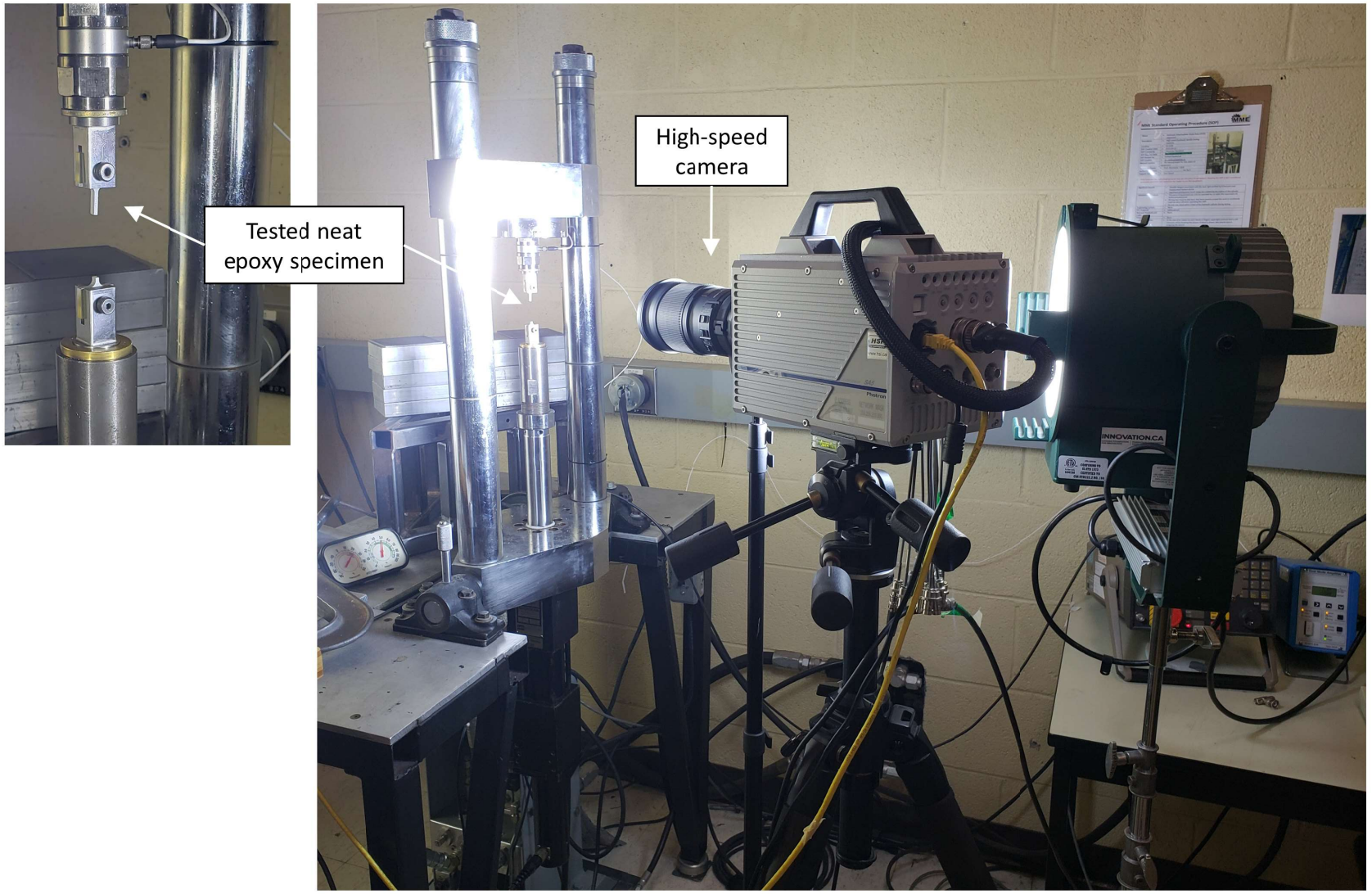
Tested neat epoxy specimen
High-speed camera

Laminate view

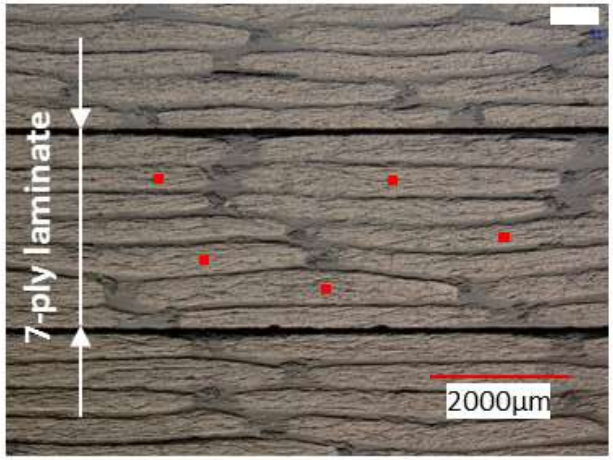

Resin-rich zones and tows

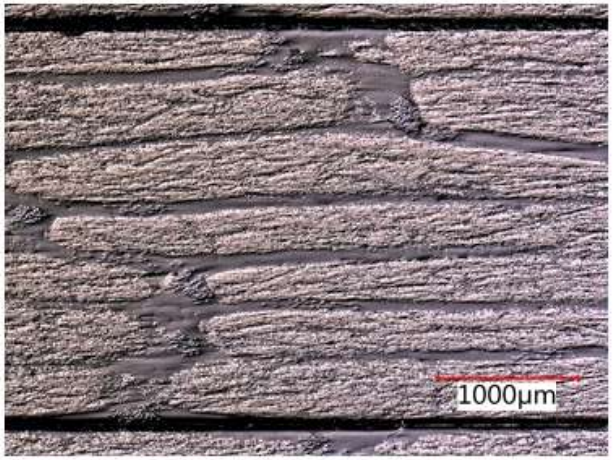

Resin-rich zones at tow-ends

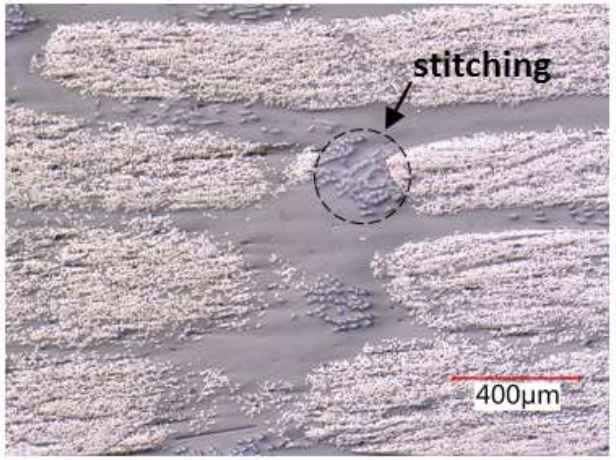

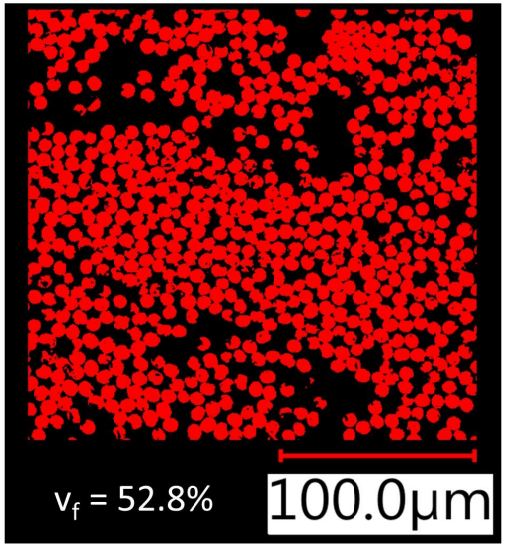
v_f = 52.8%
100.0µm

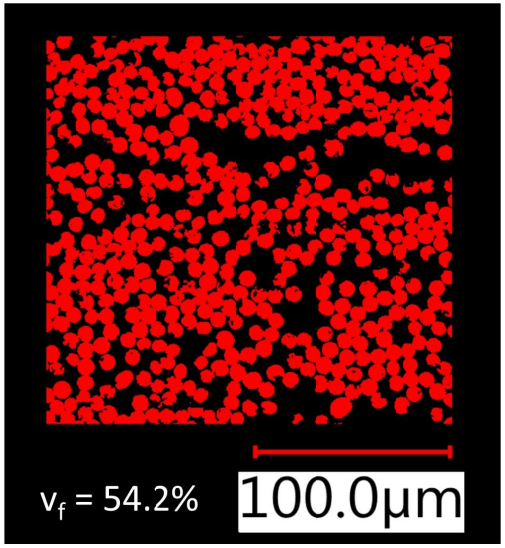
v_f = 54.2%
100.0µm

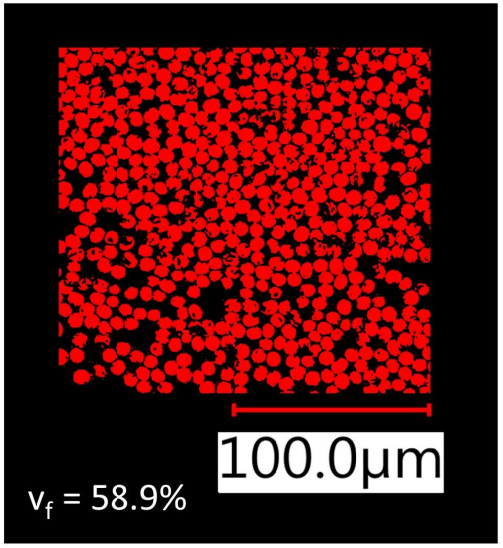
v_f = 58.9%
100.0µm

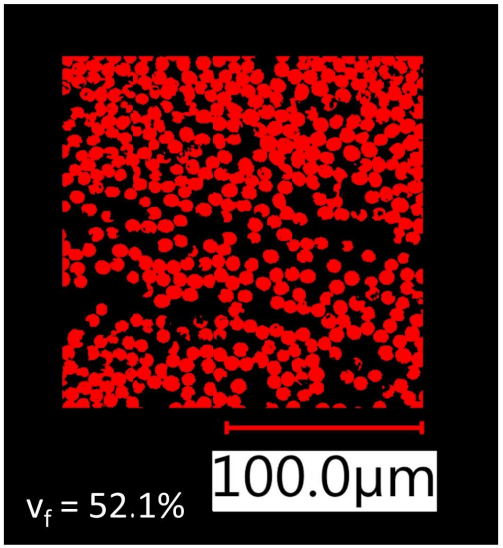
v_f = 52.1%
100.0µm

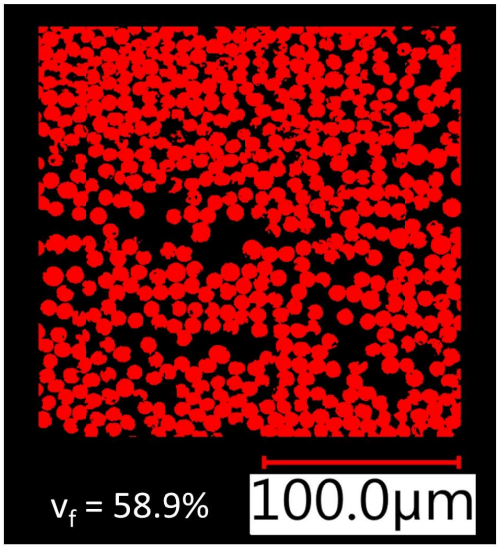
v_f = 58.9%
100.0µm

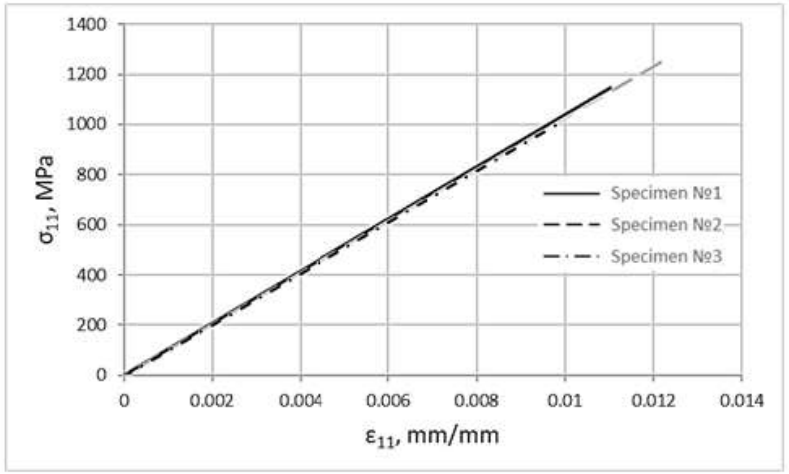
1400
1200
1000
800
600
400
200
0
σ11, MPa
0
0.002
0.004
0.006
0.008
0.01
0.012
0.014
ε11, mm/mm
Specimen №1
Specimen №2
Specimen №3

(a)

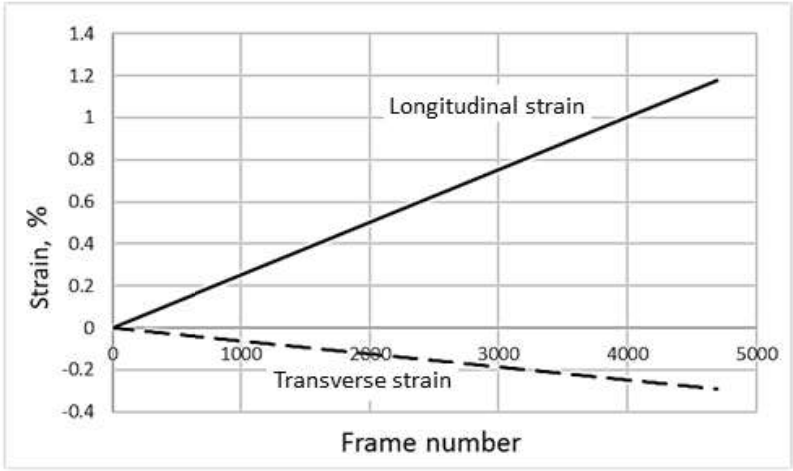
1.4
1.2
1
0.8
0.6
0.4
0.2
0
-0.2
-0.4
Strain, %
Longitudinal strain
Transverse strain
0
1000
2000
3000
4000
5000
Frame number

(b)

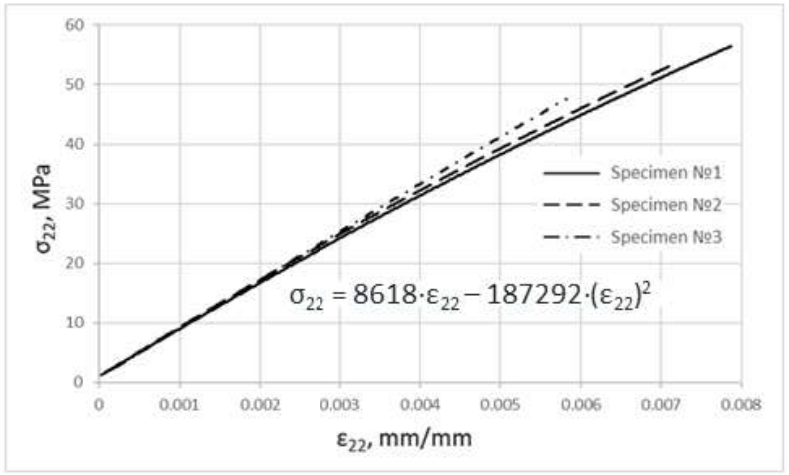
60
50
40
30
20
10
0
σ22, MPa
0
0.001
0.002
0.003
0.004
0.005
0.006
0.007
0.008
ε22, mm/mm
Specimen №1
Specimen №2
Specimen №3
σ22 = 8618·ε22 − 187292·(ε22)2

(c)

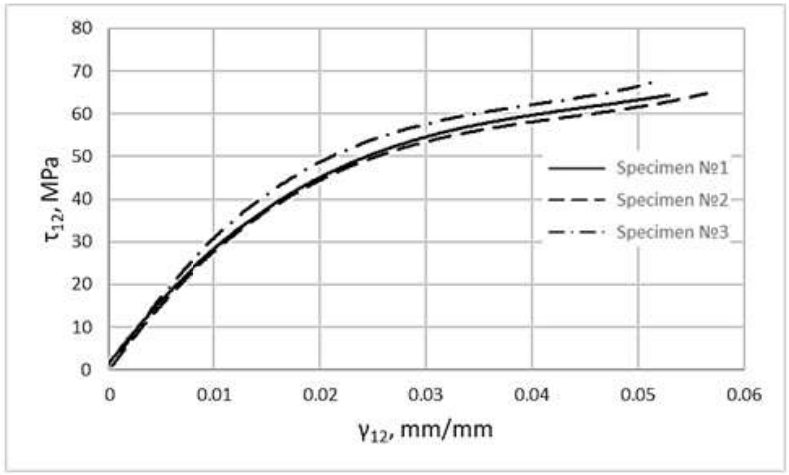
80
70
60
50
40
30
20
10
0
τ12, MPa
0
0.01
0.02
0.03
0.04
0.05
0.06
γ12, mm/mm
Specimen №1
Specimen №2
Specimen №3

(d)

Rectangular rosette

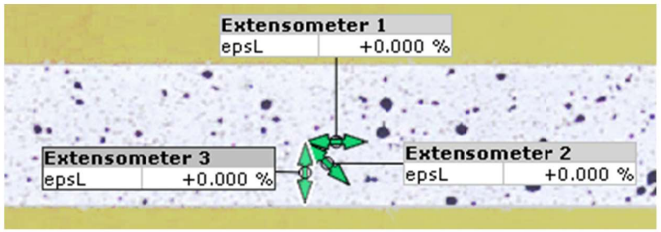

60-degree rosette

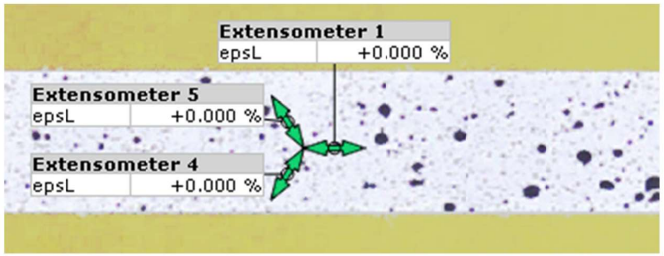

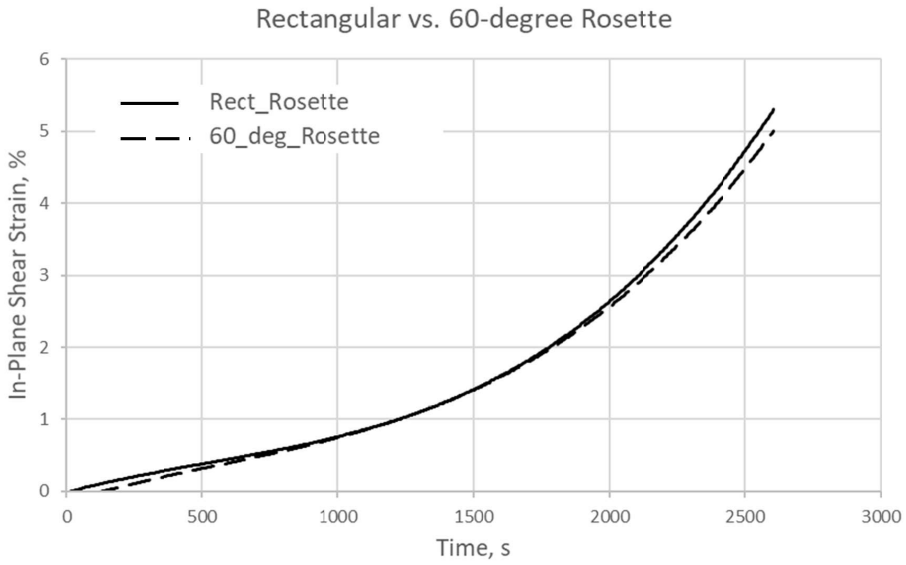

Failure mode

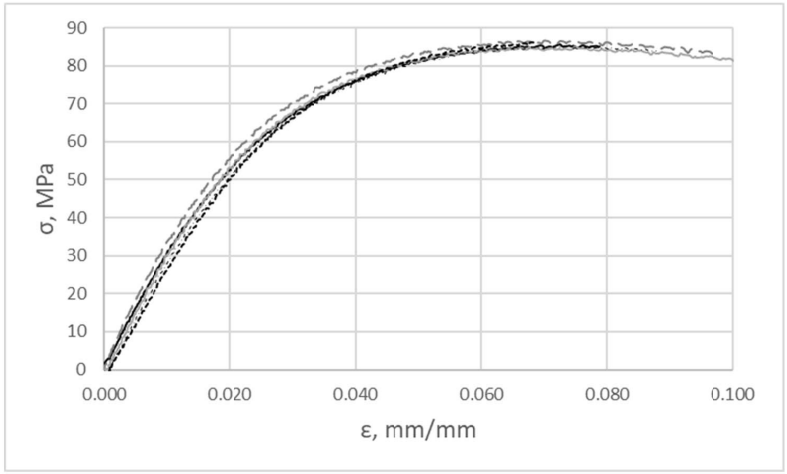
90
80
70
60
50
40
30
20
10
0
σ, MPa
0.000
0.020
0.040
0.060
0.080
0.100
ε, mm/mm

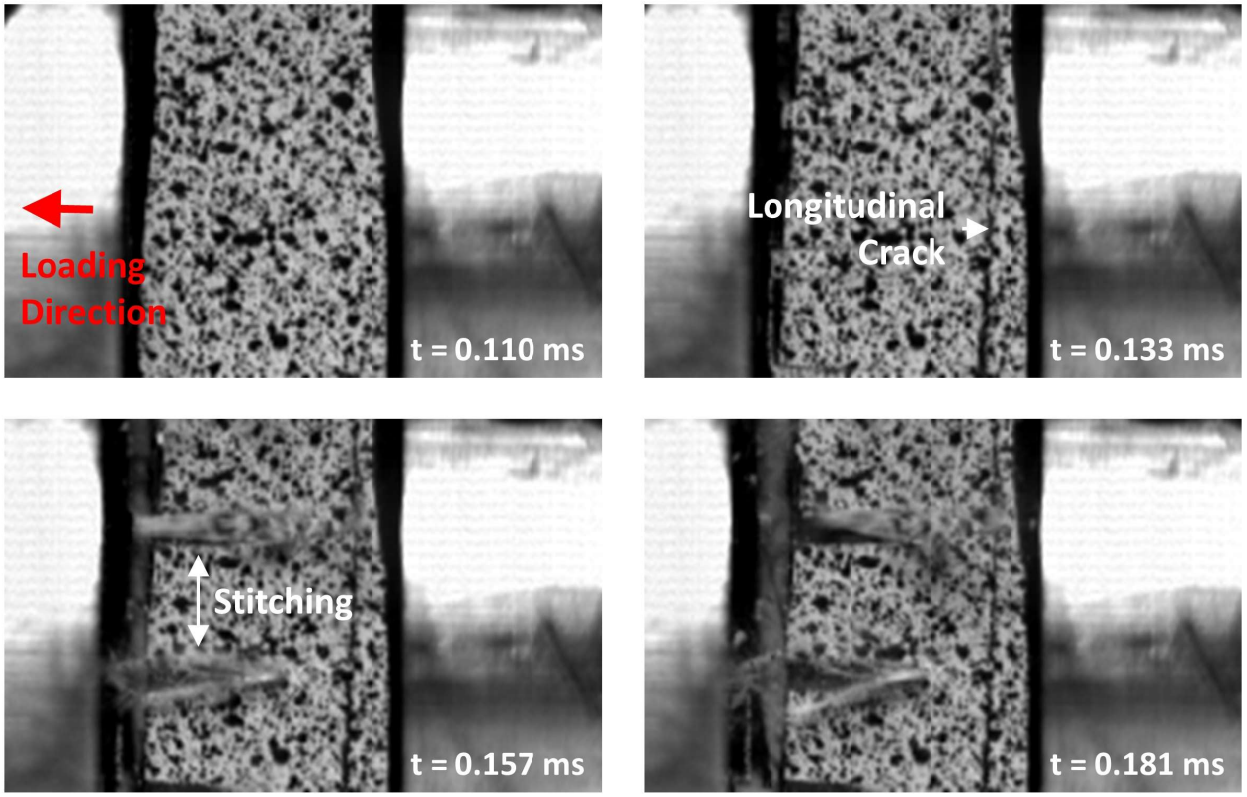
Loading
Direction
t = 0.110 ms
Longitudinal
Crack
t = 0.133 ms
Stitching
t = 0.157 ms
t = 0.181 ms

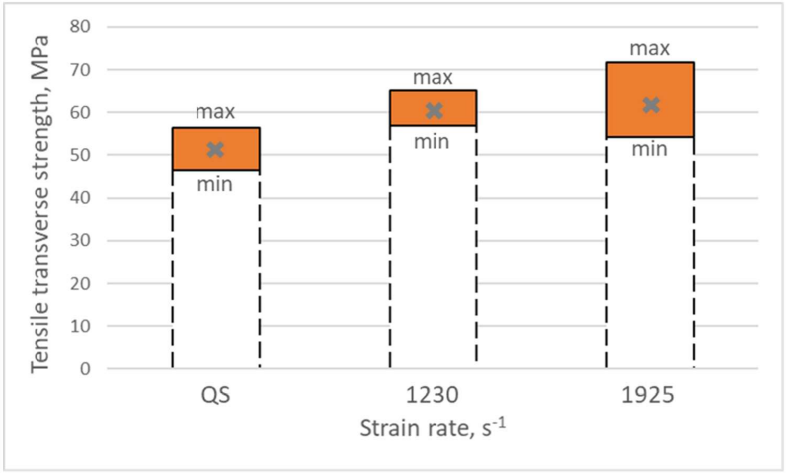
Tensile transverse strength, MPa
80
70
60
50
40
30
20
10
0
max
min
max
min
max
min
QS
1230
1925
Strain rate, s-1

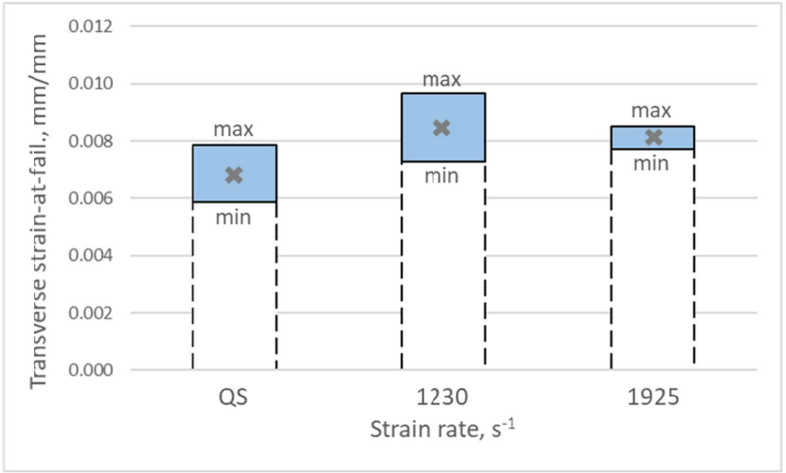
Transverse strain-at-fail., mm/mm
0.012
0.010
0.008
0.006
0.004
0.002
0.000
max
min
max
min
max
min
QS
1230
1925
Strain rate, s-1

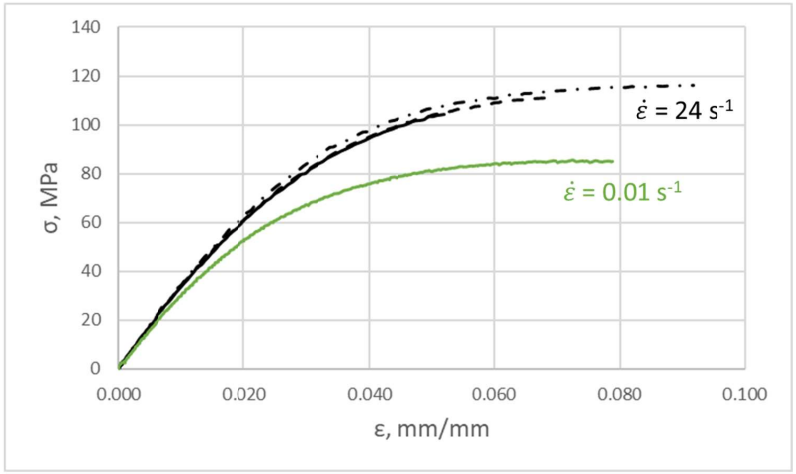
140
120
100
80
60
40
20
0
σ, MPa
0.000
0.020
0.040
0.060
0.080
0.100
ε, mm/mm
$\dot{\varepsilon}$ = 24 s^{-1}
$\dot{\varepsilon}$ = 0.01 s^{-1}